

CHEMISTRY

A European Journal

A Journal of



Accepted Article

Title: Electronic Communication in Confined Space Coronas of Shell-by-Shell Structured Al₂O₃-Nanoparticle Hybrids Containing Two Layers of Functional Organic Ligands

Authors: Andreas Hirsch and Lisa Stiegler

This manuscript has been accepted after peer review and appears as an Accepted Article online prior to editing, proofing, and formal publication of the final Version of Record (VoR). This work is currently citable by using the Digital Object Identifier (DOI) given below. The VoR will be published online in Early View as soon as possible and may be different to this Accepted Article as a result of editing. Readers should obtain the VoR from the journal website shown below when it is published to ensure accuracy of information. The authors are responsible for the content of this Accepted Article.

To be cited as: *Chem. Eur. J.* 10.1002/chem.201901052

Link to VoR: <http://dx.doi.org/10.1002/chem.201901052>

Supported by
ACES

WILEY-VCH

Electronic Communication in Confined Space Coronas of *Shell-by-Shell* Structured Al₂O₃-Nanoparticle Hybrids Containing Two Layers of Functional Organic Ligands

Lisa M. S. Stiegler^[a] and Andreas Hirsch^{*[a]}

Abstract: A first series of examples for confined space interactions of electron-rich and electron-poor molecules organized in an internal corona of *shell-by-shell* (*SbS*)-structured Al₂O₃-NP-hybrids is reported. The assembly concept of the corresponding hierarchical architectures relies on both, covalent grafting of phosphonic acids on the NPs surface (SAMs formation), and exohedral interdigitation of orthogonal amphiphiles as second ligand layer driven by solvophobic interactions. The electronic communication between the chromophores of different electron demand, such as pyrenes, PDIs (with and without pyridinium-bromide headgroups) and fullerenes was promoted at the layer interface. We have demonstrated that the efficient construction principle of the bilayer hybrids assembled around the electronically "innocent" Al₂O₃ core is robust enough to achieve control over electronic communication between electron-donors and –acceptors in the interlayer region. The electronic interactions between the electron-accepting and electron-donating moieties approaching each other at the layer interface were monitored by fluorescence measurements.

Introduction

We have recently introduced a new concept – the so-called *shell-by-shell* (*SbS*) coating method – which allows for the assembly of unprecedented nanoparticles (NPs) coated with two layers of organic ligands.^[1] The binding of the first ligand shell was carried out by covalent attachment of an organic molecule bearing a phosphonic acid terminus. This allows for efficient grafting to the surface of metal oxide NPs resulting in the formation of densely packed self-assembled monolayers (SAMs).^[2] In a second step this first-shell functionalized NPs were converted into a bilayer architecture by non-covalent interdigitation of amphiphiles forming the second layer. As a consequence, a micellar-like arrangement around the first-shell functionalized NPs was formed. The only example of a somewhat related concept involves an amphiphilic polymeric shell to hydrophobic coated nanocrystals.^[3] Such a construction of a hierarchically ordered core-shell system is driven by solvophobic interactions. Inspired is the *shell-by-shell* coating concept by the *layer-by-layer* (*LbL*) approach, firstly described by Decher et al.^[4] The layer-by-layer technique describes a concept, where substrates are alternately immersed

into charged polymer solutions to built-up multilayer assemblies onto substrates by employing electrostatic interactions between oppositely charged building blocks.

In a recent project, we manufactured Al₂O₃ NPs with mixed shells consisting of three phosphonic acid derivatives with different polarities in combination with a pyrene-terminated phosphonic acid.^[5] For these systems, the optoelectronic properties of the pyrene core in a series of environments were investigated by fluorescence spectroscopy investigations. Furthermore, we have attached different types of amphiphiles onto the corresponding first-shell-systems, which caused the embedding of pyrene chromophores in a defined environmental corona around the NPs. This allowed for tuning of the optical properties (fluorescence behavior). In general, our *SbS*-concept offers very exciting opportunities for the investigation of chemical and physical processes in a confined space, namely the interface between the two organic layers.

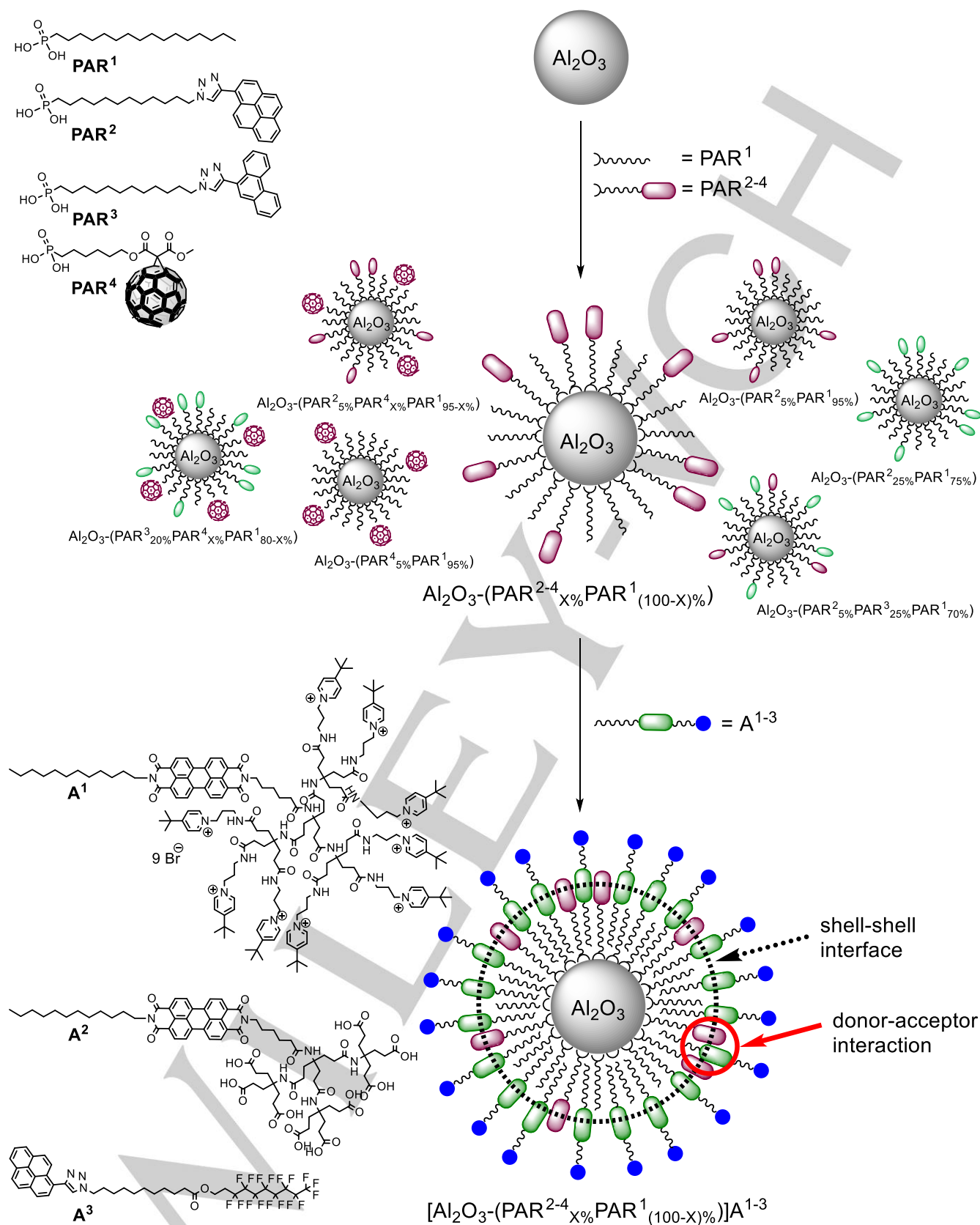
Herein, we report on a first series of examples for the successful realization of this idea. We developed *SbS*-structured Al₂O₃-NP-hybrids, where electronic communication between various chromophores of different electron demand can be promoted at the layer interface. We have demonstrated that the efficient construction principle of the bilayer hybrids assembled around the electronically "innocent" Al₂O₃ core is robust enough to achieve control over electronic communication between electron-donors and –acceptors in the interlayer region. The composition of the corresponding micellar arrangements is depicted in Scheme 1. The electronic interactions between the electron-accepting and electron-donating moieties approaching each other at the layer interface were monitored by fluorescence measurements.

For the synthesis of the targeted micellar nano-hybrids, Al₂O₃-NPs were functionalized both with long chain phosphonic acids (PAR¹) acting as isolating spacers and with functional, electron donor bearing phosphonic acids PAR²⁻³ in different ratios. Employing a combination of both pyrene and/or phenanthrene containing ligands (PAR² and PAR³) together with an electron accepting phosphonic acid involving C₆₀ (PAR⁴) leads to a fluorescence quenching. This is an indication of pronounced donor-acceptor (EDA) complex formation^[6] events in the first ligand shell. PAR¹ was also combined with PAR² and/or PAR³ in the first shell, together with the electron-accepting perylenediimides A¹ and A² (with either pyridinium-bromide or carboxylic acid head groups) in the second shell. The apolar tails of the amphiphiles were incorporated into the first-shell system, whereas the polar head groups were pointing outwards.^[7] At the shell-shell interface, donor-acceptor complexation of the pyrene and/or phenanthrene (PAR²/PAR³) together with the PDI-cores occurs, which was figured out by quenching fluorescence measurements. An additional push-pull system was built-up by

[a] L. M. S. Stiegler, Prof. Dr. A. Hirsch
Chair of Organic Chemistry II, Department of Chemistry & Pharmacy
Friedrich-Alexander-Universität Erlangen-Nürnberg
Nikolaus-Fiebiger-Strasse 10, 91058 Erlangen (Germany)
E-mail: andreas.hirsch@fau.de

Supporting information for this article is given via a link at the end of the document.

FULL PAPER



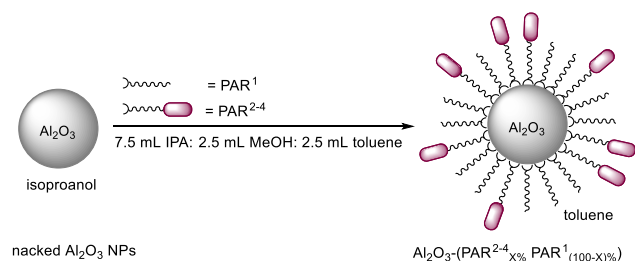
Scheme 1. General *shell-by-shell* functionalization approach of aluminium oxide NPs with a mixture of PAR^1 and PAR^{2-4} as first ligand shell and the amphiphiles A^{1-3} as second supramolecular ligand shell promoting electronic communication between donor- and acceptor chromophores in the confined space of the shell-shell interface.

FULL PAPER

the combination of PAR¹ together with the electron-poor C₆₀ in the first shell and with the electron-rich pyrene amphiphile (A³) in the second shell in fluorinated solvents. The core-shell(-shell) NPs were further investigated by UV-Vis measurements, thermogravimetric analysis (TGA), Fourier transform infrared spectroscopy (FTIR), DLS and Zeta-potential characterization.

Results and Discussion

For the *shell-by-shell* coating procedure dispersions of Al₂O₃ NPs with a specific surface area of 109 m²g⁻¹ and an average diameter of 14 nm, as determined in BET measurements, were used. As dispersion medium isopropanol was used. The treatment of the parent alumina NPs with phosphonic acids bearing lipophilic moieties PAR¹-PAR⁴ afforded the densely coated NPs Al₂O₃-(PAR²⁻⁴_{X%} PAR¹_{(100-X)%}) (Scheme 2).

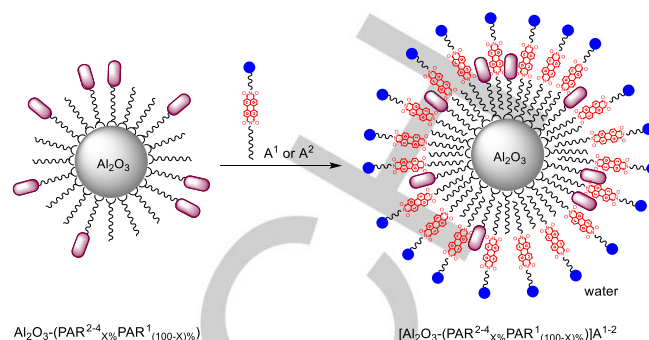


Scheme 2. Covalent surface functionalization of aluminium oxide NPs with different ratios of phosphonic acids PAR¹⁻⁴ to generate Al₂O₃-(PAR²⁻⁴_{X%} PAR¹_{(100-X)%}) NPs, in particular Al₂O₃-(PAR²⁻⁴_{5%} PAR¹_{(95-X)%}), Al₂O₃-(PAR^{3-20%} PAR^{4-X%} PAR¹_{(80-X)%}) (with X = 0-10), Al₂O₃-(PAR^{2-5%} PAR¹_{95%}), Al₂O₃-(PAR^{3-25%} PAR¹_{75%}), Al₂O₃-(PAR^{2-5%} PAR^{3-25%} PAR¹_{70%}), or Al₂O₃-(PAR^{4-5%} PAR¹_{95%}).

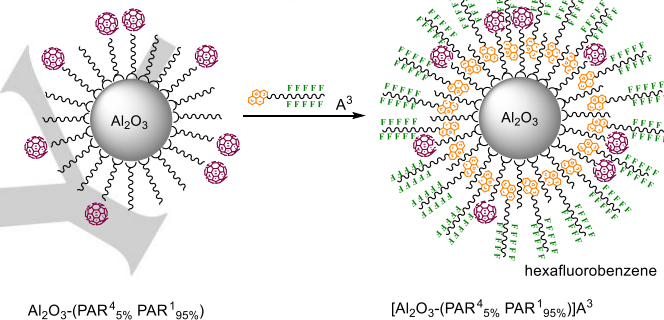
For the functionalization procedure of Al₂O₃ NPs, the phosphonic acids PAR²⁻⁴ were mixed in different ratios with PAR¹ to adjust the packing density of the chromophores PAR²⁻⁴ on the NP-surface and to prevent that the chromophores come too close to each other, which would result in a shift of the monomer band to the excimer band of PAR² in the fluorescence spectra.

After this procedure the dispersibility moved from isopropanol to apolar solvents, like toluene. The monolayer coated NPs Al₂O₃-(PAR²⁻⁴_{X%} PAR¹_{(100-X)%}) were isolated and purified by repeated centrifugation and redispersion in isopropanol and finally in toluene. Subsequently the mono-shell functionalized NPs were subjected to a second in this case non-covalent functionalization by treatment with the amphiphiles A¹, A², or A³ and simultaneous dispersion of the reaction products [Al₂O₃-(PAR²⁻⁴_{X%} PAR¹_{(100-X)%})]A¹⁻³ in water or hexafluorobenzene, respectively (Scheme 3 and 4). During this procedure a polarity umpolung induced by the second ligand shell takes place according to the new supramolecular construction concept that we reported recently.^[1b, 1c, 5] As a result a micellar arrangement was formed involving lipophilic interactions between the apolar parts (R¹-R⁴) of the first layer and the lipophilic termini of A¹⁻³. The major driving force for the straightforward assembly of [Al₂O₃-(PAR²⁻⁴_{X%} PAR¹_{(100-X)%})]A¹⁻³ are solvophobic interactions. With the choice of the first shell ligands PAR¹⁻⁴ and the second shell amphiphiles A¹⁻³ we developed a library of non-functional (PAR¹) and functional building blocks containing electron-rich components such as phenanthrene and pyrene (PAR^{2,3}, A³) or electron-accepting units

such as fullerene C₆₀ (PAR⁴), perylene (A²) and perylene/pyridinium (A³).



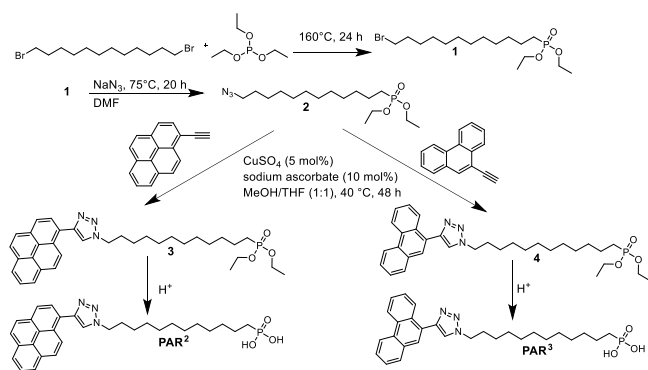
Scheme 3. *Shell-by-shell* functionalization of mono-shell NPs Al₂O₃-(PAR²⁻⁴_{X%} PAR¹_{(100-X)%}) with the amphiphiles A¹ or A², resulting in [Al₂O₃-(PAR²⁻⁴_{X%} PAR¹_{(100-X)%})]A¹⁻².



Scheme 4. *Shell-by-shell* functionalization of mono-shell NPs Al₂O₃-(PAR^{4-5%} PAR¹_{95%}) with the amphiphile A³, resulting in [Al₂O₃-(PAR^{4-5%} PAR¹_{95%})]A³.

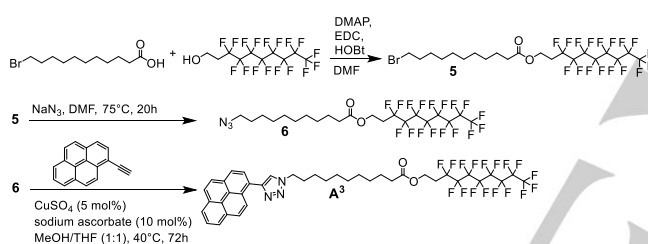
Permutations of such building blocks in the first and second ligand shell will allow for enabling or disabling electronic communication at the ligand shell interfaces. These types of highly integrated functional architectures are unprecedented. Whereas compounds PAR^{1,4} and A^{1,2} are known, synthetic access to PAR^{2,3} and A³ had been established.^[8] The stepwise synthesis of the new phosphonic-acid derivatives PAR² and PAR³ is outlined in scheme 5. The precursor molecule **1** was synthesized by a Michaelis-Arbuzov reaction of 1,12-dibromododecane with triethylphosphite in 25.6% yield. Compound **2** was generated by a nucleophilic substitution of the bromide substituent in **1** with sodium azide in 95.9% yield. The azide functionality of the phosphonate-ester was subsequently subjected to “click” reactions^[9] with 1-ethynylpyrene or 9-ethynylphenanthrene leading to the formation of **3** in 31.4% yield and **4** in 34.1% yield. Final deprotection afforded the target molecules PAR² in 91.0% yield and PAR³ in 92.8% yield.

FULL PAPER



Scheme 5. Synthetic procedures towards phosphonic acids PAR² and PAR³.

The synthesis of A³ is shown in scheme 6. The initial step was a Steglich-coupling of 11-bromoundecanoic acid with 1*H*, 1*H*, 2*H*, 2*H*-perfluoro-1-decanol leading to compound **5** in 42.5% yield. In the next step, molecule **5** was converted to the azide **6** by a nucleophilic substitution reaction of bromide affording the azide in 80.3% yield. In the final stage a “click” reaction to the azide group of **6** with 1-ethynylpyrene led to the target amphiphile **A**³ in 53.1% yield.



Scheme 6. Synthetic procedure towards amphiphile A³.

As an example to prove the successful functionalization of Al₂O₃ NPs, a phosphonic acid mixture of 5% PAR² and 95% PAR¹ was used, TGA measurements were performed with particles functionalized with different concentrations (0.2 – 7.0 mM) of the phosphonic-acid mixture (see Figure 1).^[10] This ratio of phosphonic acids was used frequently in the following procedures because it provides excellent fluorescence properties with a predominant monomer fluorescence band of the pyrene unit and minor excimer fluorescence, only. Moreover, the pyrene chromophores, gives rise to a characteristic absorbance in the UV-Vis spectra. With increasing phosphonic acid (PA) concentrations the weight loss raises until a plateau is reached at 3 mM PA indicating the saturation of binding due to complete surface coverage. With the grafting densities determined from the weight loss of the cleaved ligands, a Langmuir isotherm could be obtained. Such a behavior has been demonstrated to reflect successful monolayer functionalization.^[1a, 11] By plotting the reciprocal values of the grafting densities versus reciprocal concentrations of the phosphonic acid mixtures, a linear fit was applied. From the intercept of the linear fit the maximum monolayer grafting density was determined to be 3.62 molecules/nm². (For more information see Figure S2 (SI)). This value is in good agreement with a literature example, where an alumina surface was treated with *n*-octadecylphosphonic acid

leading to a packing density of 4.6 molecules per nm², as determined by XPS analysis.^[12]

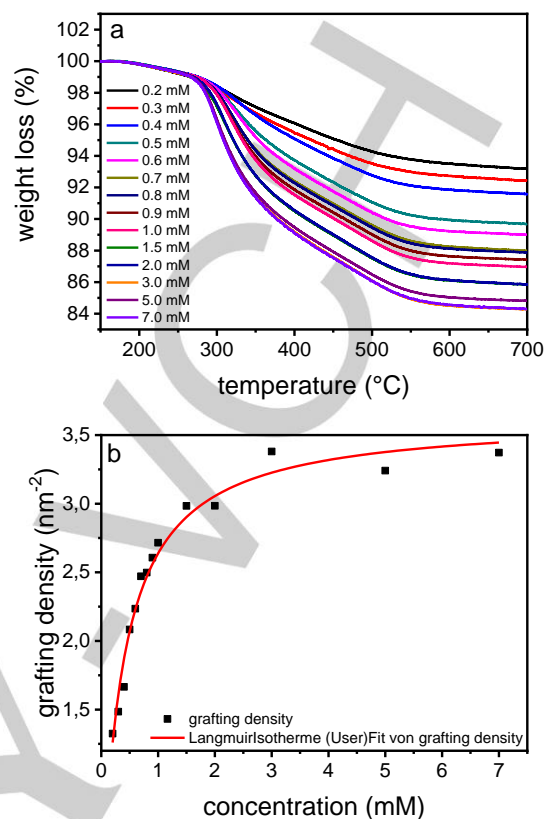


Figure 1. (a) TGA weight-loss curve of Al₂O₃-(PAR²_{5%} PAR¹_{95%}) as a function of the PA concentration maintaining a ratio of 95% PAR² and 5% PAR¹ and (b) the corresponding Langmuir isotherm indicating monolayer coverage.

After the proof of successful monolayer-functionalization leading to Al₂O₃-(PAR²_{5%} PAR¹_{95%}), we targeted the synthesis of hybrid architectures where both electron rich and electron poor PA-derivatives form the first ligand shell. For this purpose the alumina NPs were treated with 5% PAR², X% PAR⁴, and (95-X)% PAR¹ mixtures of the PAs (with X = 0-10) in order to perform systematic studies on the ratio-dependent fluorescence quenching of the pyrene functionality caused by the C₆₀ chromophore.^[13] The corresponding core shell hybrids Al₂O₃-(PAR²_{5%} PAR¹_{95%}) without fullerene (X = 0) give rise to a pronounced pyrene fluorescence in toluene at an irradiation wavelength of λ_{max} = 288 nm. With an increasing amount of PAR⁴ (X > 0) the fluorescence of the pyrene-functionality was successively quenched due to the interaction with the electron-accepting fullerene core in close and fixed proximity on the NP-surface (see Figure 2a). At the same time, the characteristic absorption of the C₆₀ chromophore at λ_{max} = 270 nm increased in intensity (Figure S7a). The same investigation was carried out for the composition of 20% PAR³, X% PAR⁴, and (80-X)% PAR¹ (X = 0-10). It could be clearly demonstrated that also the phenanthrene fluorescence at λ_{max} = 381 nm decreased stepwise with increasing amount of the C₆₀ containing PAR⁴ in the first ligand shell (see Figure 2b and Figure S7b). Again the reason for the tailorable fluorescence quenching is an electron donor-acceptor (EDA) complex formation between the polycyclic

FULL PAPER

aromatic hydrocarbon donor and the fullerene acceptor in the first layer interface.^[14]

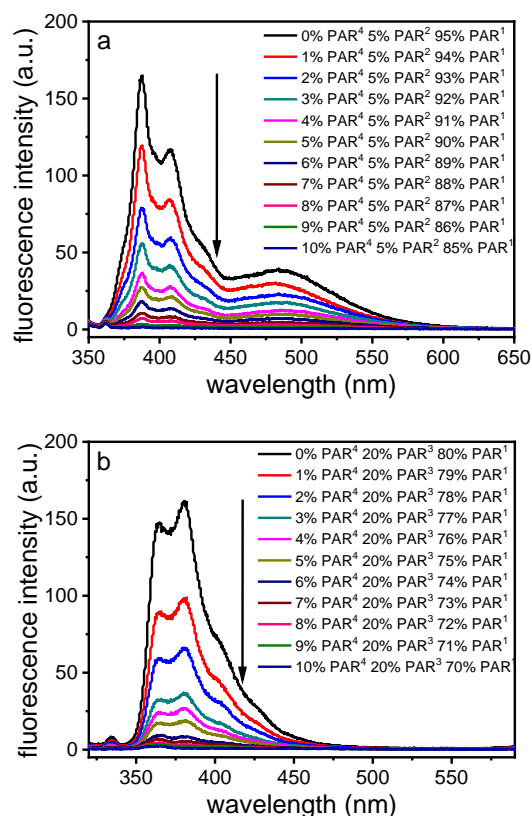
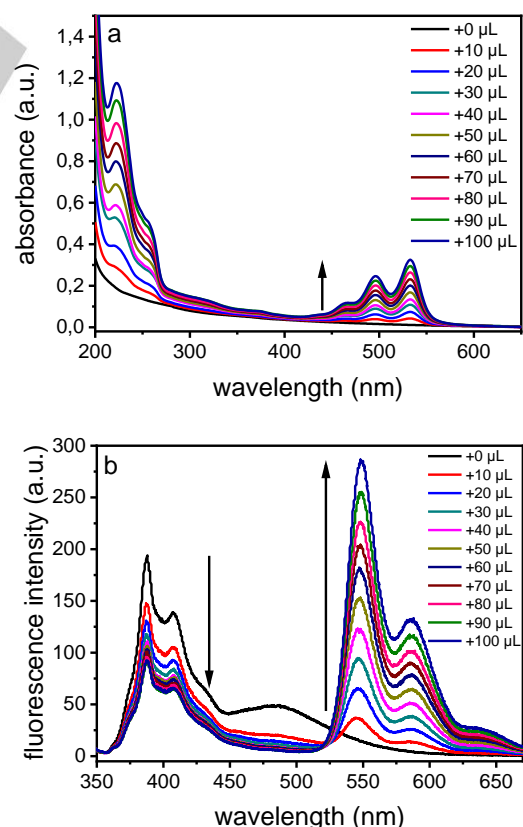


Figure 2. Fluorescence quenching behaviour of (a) $\text{Al}_2\text{O}_3\text{-(PAR}^{2.5\%}\text{ PAR}^{4x\%}\text{ PAR}^{1(95-x)\%})$ ($\lambda_{\text{ext}} = 340\text{ nm}$) and (b) $\text{Al}_2\text{O}_3\text{-(PAR}^{3.20\%}\text{ PAR}^{4x\%}\text{ PAR}^{1(80-x)\%})$ ($\lambda_{\text{ext}} = 300\text{ nm}$).

To reach the next hierarchical level amphiphilic perylene diimides A^{1-2} were now connected to $\text{Al}_2\text{O}_3\text{-(PAR}^{2-4x\%}\text{ PAR}^{1(100-x)\%})$ generating the second ligand shell. As a first prototype we studied the formation of $[\text{Al}_2\text{O}_3\text{-(PAR}^{2.5\%}\text{ PAR}^{1.95\%})]\text{A}^1$. The formation of this supramolecular construct is driven by hydrophobic interactions between the alkyl chain of A^1 and the apolar first ligand shell of $\text{Al}_2\text{O}_3\text{-(PAR}^{2.5\%}\text{ PAR}^{1.95\%})$. It was expected that the donor-acceptor interactions between the pyrenes of the first ligand shell and the electron-poor perylene diimides^[15] or pyridinium termini of the second ligand shell will be established. For this purpose, we investigated the changing optical features of $\text{Al}_2\text{O}_3\text{-(PAR}^{2.5\%}\text{ PAR}^{1.95\%})$ as a function of added A^1 . In detail, 2 mL of the suspended $\text{Al}_2\text{O}_3\text{-(PAR}^{2.5\%}\text{ PAR}^{1.95\%})$ in water was titrated in 10 μL steps with $[\text{Al}_2\text{O}_3\text{-(PAR}^{2.5\%}\text{ PAR}^{1.95\%})]0.2\text{ mM A}^1$ in water to make sure that the concentration of alumina oxide NPs and pyrene-functionality was constant during the titration experiment and no diluting effects occur. With this procedure we covered a concentration range of A^1 from 0-0.22 mM. During the titration the absorbance of A^1 at $\lambda_{\text{max}} = 533\text{ nm}$ increased with an increasing amount of A^1 (Fig. 3a). Particle dispersions were irradiated with a laser at an excitation wavelength of 340 nm, causing an exponential decrease of pyrene fluorescence (see Figure 3c). On the other, the perylene diimide chromophore A^1 started to emit light at $\lambda_{\text{max}} = 550\text{ nm}$ (Figure 3b,d). The decrease of the pyrene fluorescence is a proof for a successful electron communication between the electron-rich pyrene and the

electron-poor perylene diimide/pyridinium bromide. Amphiphile A^1 consists of two different electron accepting functionalities, namely a PDI core, which is a strong electron acceptor,^[16] and pyridinium substituents, which can also act as moderate electron acceptors and which can facilitate photoinduced electron transfer (PET) reactions.^[17] Moreover, they have been demonstrated to be efficient quenchers for the fluorescence of alternant polycyclic-aromatic hydrocarbons.^[18] After the first titration step, resulting in the consumption of 0.001 mM A^1 , the fluorescence quenching of the pyrene-functionality was most significant and also the excimer-fluorescence was fully disintegrated. Both phenomena indicate that the amount of added A^1 was high enough to establish a fully-covered second-shell around $\text{Al}_2\text{O}_3\text{-(PAR}^{2.5\%}\text{ PAR}^{1.95\%})$. The dodecyl-chains of A^1 interdigitate the lipophilic area of the first-shell functionalized NPs *via* hydrophobic interactions and weakened the pyrene excimer-complex formation^[19] on the surface. After full coverage of the second shell with A^1 , spatially seen, additional interactions with A^1 present in the NP dispersion causes less electronic interaction with the pyrene-units. This can also be explained by appearance of an exponential decay of the quenched pyrene fluorescence. After the first titration step, generating a nearly full covered second shell, further quenching is less pronounced, because of sterically hindered interaction of A^1 with the pyrene-units. Moreover, the terminating polar pyridinium headgroups of $[\text{Al}_2\text{O}_3\text{-(PAR}^{2.5\%}\text{ PAR}^{1.95\%})]\text{A}^1$ provided excellent dispersibility in water and stabilized the initial lipophilic and hydrophobic first-shell functionalized nanoparticles that were suspended in water and lacked long-term stability, before titration with A^1 was carried out.



FULL PAPER

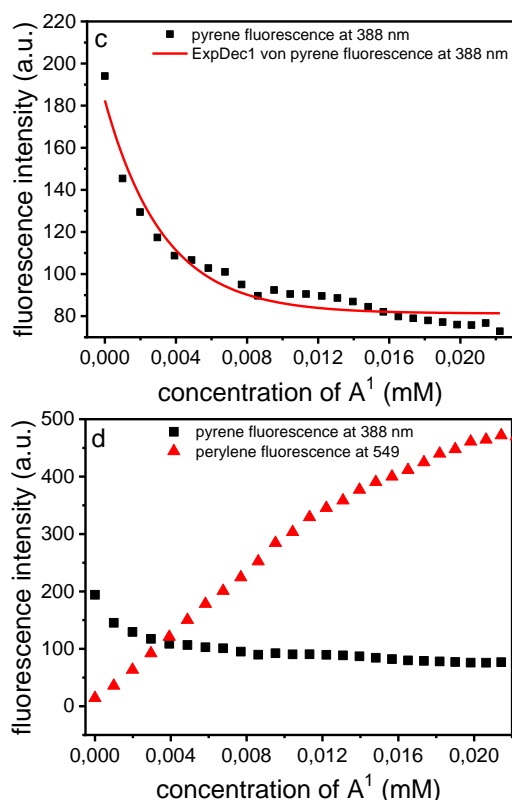


Figure 3. (a) UV-Vis and (b) fluorescence spectra of $\text{Al}_2\text{O}_3\text{-(PAR}^{2.5\%}\text{ PAR}^{1.95\%})$ titrated with A^1 in DIW, (c) exponential decay of the pyrene fluorescence in dependence on the concentration of A^1 and (d) decreased pyrene fluorescence vs. increased perylene fluorescence as a function of the concentration of A^1 ($\lambda_{\text{exc}} = 340\text{ nm}$).

The fluorescence quenching of the pyrene-functionality with A^1 can also clearly be seen from the visual appearance of the corresponding dispersions themselves. Figure 4 shows the lipophilic $\text{Al}_2\text{O}_3\text{-(PAR}^{2.5\%}\text{ PAR}^{1.95\%})$ particles in the upper toluene-phase. The lower aqueous-phases (on the right side each) contain the hydrophilic $[\text{Al}_2\text{O}_3\text{-(PAR}^{2.5\%}\text{ PAR}^{1.95\%})]\text{A}^1$ NPs. The first-shell functionalized NPs $\text{Al}_2\text{O}_3\text{-(PAR}^{2.5\%}\text{ PAR}^{1.95\%})$ are colorless and nearly transparent, whereas second-shell functionalized NPs $[\text{Al}_2\text{O}_3\text{-(PAR}^{2.5\%}\text{ PAR}^{1.95\%})]\text{A}^1$ appear pink at day-light (Figure 4a). Under UV-light (Figure 4b), first-shell functionalized NPs $\text{Al}_2\text{O}_3\text{-(PAR}^{2.5\%}\text{ PAR}^{1.95\%})$ reveal a turquoise fluorescence that is quenched by A^1 .

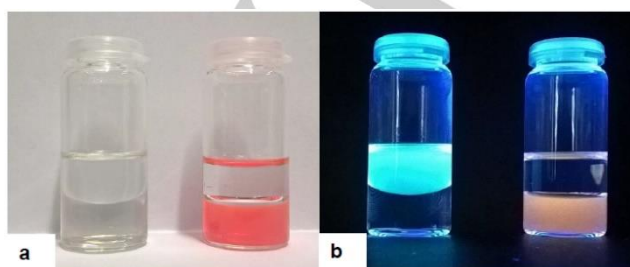


Figure 4. Dispersibility behaviour and optical properties of $\text{Al}_2\text{O}_3\text{-(PAR}^{2.5\%}\text{ PAR}^{1.95\%})$ in toluene (upper phase) and *shell-by-shell* functionalized NPs $[\text{Al}_2\text{O}_3\text{-(PAR}^{2.5\%}\text{ PAR}^{1.95\%})]\text{A}^1$ in DIW (lower phase) (a) under day-light and (b) under UV-light.

$\text{Al}_2\text{O}_3\text{-(PAR}^{2.5\%}\text{ PAR}^{1.95\%})$ NPs were also further functionalized with A^2 (Figure 5) in analogy to the previous case. For this purpose, 2 mL of $\text{Al}_2\text{O}_3\text{-(PAR}^{2.5\%}\text{ PAR}^{1.95\%})$ NPs in water were titrated with $[\text{Al}_2\text{O}_3\text{-(PAR}^{2.5\%}\text{ PAR}^{1.95\%})]\text{A}^2$ 0.2 mM A^2 in 10 μL steps. Whereas the UV-Vis absorbance of A^2 at $\lambda_{\text{max}} = 473\text{ nm}$ increased with an increasing amount of the PDI (Figure 5a), the fluorescence of the pyrene-functionality decreased during the titration (Figure 5b,d). The monomer-fluorescence of the pyrene functionality at $\lambda_{\text{max}} = 388\text{ nm}$ decreased slowly, while the excimer formation around 488 nm decreased more significantly. This is a strong indication for the expected micellar-like arrangement of A^2 forming the second layer of the supramolecular NPs $[\text{Al}_2\text{O}_3\text{-(PAR}^{2.5\%}\text{ PAR}^{1.95\%})]\text{A}^2$. The long lipophilic tail of A^2 is interdigitated non-covalently into the first shell. This causes at the same the disassembly of pyrene-excimer. The supramolecular NPs $[\text{Al}_2\text{O}_3\text{-(PAR}^{2.5\%}\text{ PAR}^{1.95\%})]\text{A}^2$ were also irradiated at $\lambda_{\text{exc}} = 475\text{ nm}$, the absorption maximum of the perylene-dimide chromophore A^2 (Figure S6b). As expected, the fluorescence of A^2 at $\lambda_{\text{max}} = 686\text{ nm}$ increased during the addition of A^2 (see Figure 5c). Figure 5d displays a diagram where we plotted the decreasing pyrene-excimer fluorescence and the increasing perylene-dimide A^2 fluorescence against the concentration of A^2 . The excitation wavelength λ_{exc} was 340 nm, the region with the highest pyrene absorption. Compared to $[\text{Al}_2\text{O}_3\text{-(PAR}^{2.5\%}\text{ PAR}^{1.95\%})]\text{A}^1$, the fluorescence quenching of pyrene was weaker, and also the increase of the perylene-fluorescence. To gain more insight into the electronical communication of the first ligand shell electron-donor PAR^2 with electron acceptors A^1/A^2 located in the second ligand shell, we performed cyclic voltammetry (CV) studies as supporting reference experiments. In particular we investigated 1-dodecyl-pyridinium bromide (DDPB) as a second-shell amphiphile. The absorption and fluorescence spectra of $\text{Al}_2\text{O}_3\text{-(PAR}^{2.5\%}\text{ PAR}^{1.95\%})$ are shown in Figure S19 (SI). The analysis of the fluorescence quenching of $\text{Al}_2\text{O}_3\text{-(PAR}^{2.5\%}\text{ PAR}^{1.95\%})$ NPs as a function of the DDPB concentration reveal very similar results as those observed for $[\text{Al}_2\text{O}_3\text{-(PAR}^{2.5\%}\text{ PAR}^{1.95\%})]\text{A}^1$. The quenching of the pyrene-unit is very significant, especially after the first titration step, and with further titration steps, the quenching flattened. Overall it follows also an exponential decay, similar to the exponential decay observed for the titration with A^1 . As already mentioned, the quenching with A^2 is less efficient. Reference CV-measurements of DDPB and A^1 are shown in Figure S20 and S21 (SI). It can be seen that the pyridinium unit of DDPB is reduced at $E_{\text{red}}(\text{DDPB}) = -1,76\text{ V vs. Ag/AgCl}$, whereas molecule A^1 shows three reduction potentials. The first corresponds to the formation of the monoanion of the PDI core $E_{\text{red}}(\text{A}^1, \text{PDI monoanion}) = -0,81\text{ V vs. Ag/AgCl}$, the second to the formation of the dianion of the PDI core $E_{\text{red}}(\text{A}^1, \text{PDI dianion}) = -1,12\text{ V vs. Ag/AgCl}$ and the third reduction potential is due to pyridinium-bromide units of A^1 $E_{\text{red}}(\text{A}^1, \text{pyridinium}) = -1,72\text{ V vs. Ag/AgCl}$. Although the PDI core is the better electron acceptor, it seems, that the photo-induced electron-transfer from the pyrene-functionality to the pyridinium substituents is energetically more favorable than that of the PDI-core-only systems $[\text{Al}_2\text{O}_3\text{-(PAR}^{2.5\%}\text{ PAR}^{1.95\%})]\text{A}^2$. It appears that the pyridinium termini have a stabilizing influence on the photo-induced charge separation. Furthermore, during the titration experiment leading to the generation of $[\text{Al}_2\text{O}_3\text{-(PAR}^{2.5\%}\text{ PAR}^{1.95\%})]\text{A}^2$, A^2 is presented in its aggregated form, which could be seen in the shape of the fluorescence band^[20] that belongs to A^2 , and could also be a reason for the weaker quenching of pyrene-unit compared to the system involving A^1 .

FULL PAPER

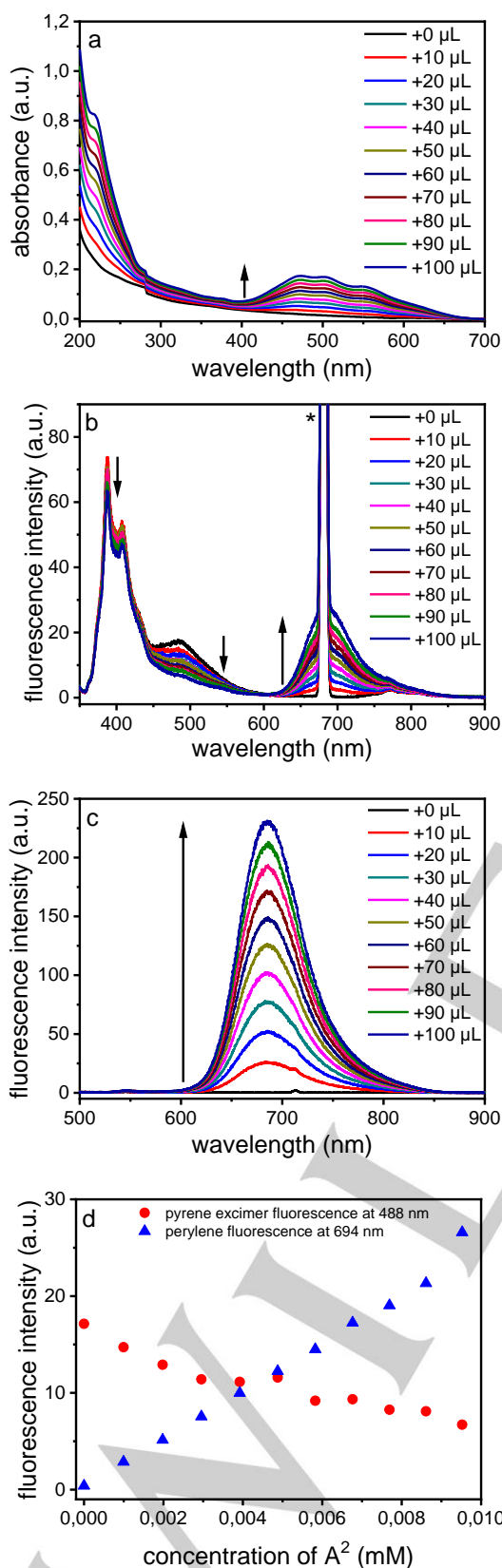
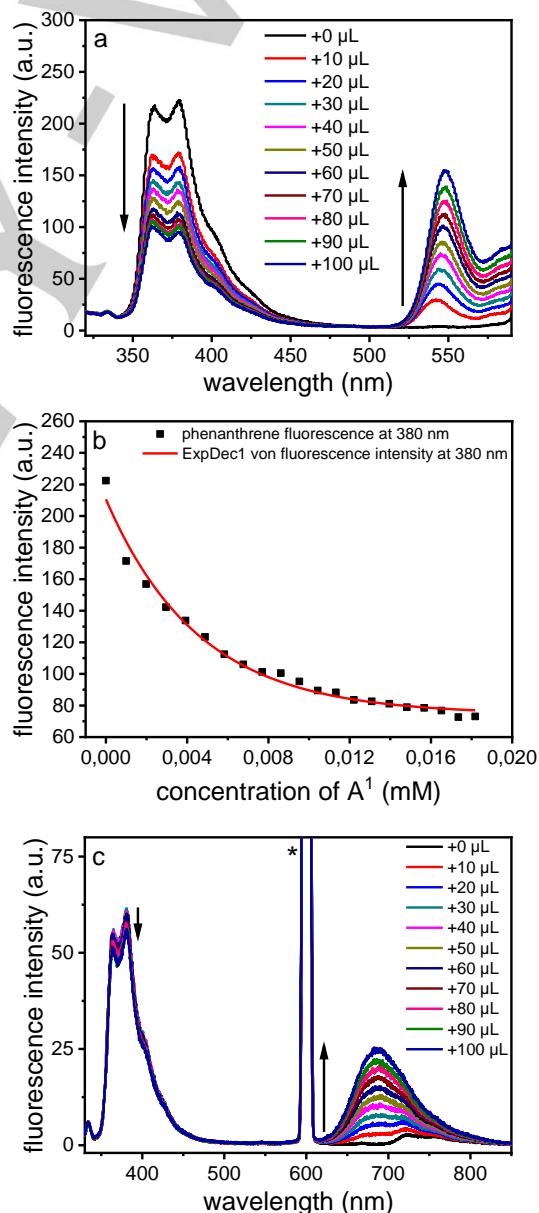


Figure 5. (a) UV-Vis and (b) fluorescence spectra of Al_2O_3 -($\text{PAR}^{25\%}$ $\text{PAR}^{195\%}$) titrated with A^2 in deionized water (DIW), $\lambda_{\text{ext}} = 340$ nm, (c) $\lambda_{\text{ext}} = 475$ nm and (d) a plot of fluorescence measurements ($\lambda_{\text{ext}} = 340$ nm) showing the quenching of

pyrene excimer fluorescence vs. increasing perylene fluorescence as a function of the concentration of A^2 .

Similar measurements were performed with the hybrids Al_2O_3 -($\text{PAR}^{3_{25\%}}$ $\text{PAR}^{1_{75\%}}$) involving PAR^3 instead of PAR^2 , to get more detailed information on the changing fluorescence properties of the electron donor PAR^3 in dependence on the electron acceptor A^1 . Figure 6a and b shows the fluorescence measurements of 2 mL Al_2O_3 -($\text{PAR}^{3_{25\%}}$ $\text{PAR}^{1_{75\%}}$) in water, titrated with $[\text{Al}_2\text{O}_3$ -($\text{PAR}^{3_{25\%}}$ $\text{PAR}^{1_{75\%}}$)]0.2mM A^1 in water and the analogous measurements using $[\text{Al}_2\text{O}_3$ -($\text{PAR}^{3_{25\%}}$ $\text{PAR}^{1_{75\%}}$)]0.2mM A^2 (Figure 8 c,d). In the case of the A^1 titration the initial fluorescence quenching is very pronounced expressed by an exponential decay of the phenanthrene fluorescence at $\lambda_{\text{max}} = 380$ nm (Figure 6b), while the perylene fluorescence at $\lambda_{\text{max}} = 549$ nm increased with an increasing amount of A^1 (Figure 6a). In the case of the titration with A^2 the phenanthrene fluorescence decreased gradually, whereas the fluorescence of A^2 starts to increase linearly.



FULL PAPER

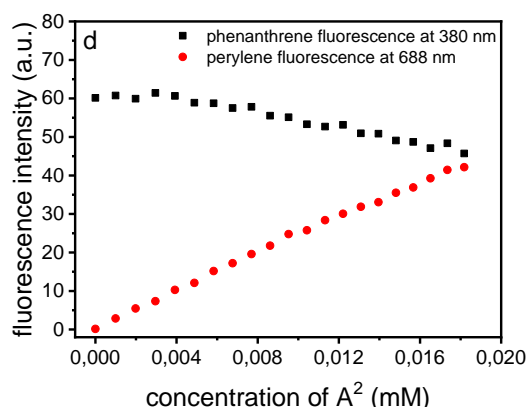


Figure 6. (a) Fluorescence spectra of Al_2O_3 -($\text{PAR}^{3_{25\%}}$ $\text{PAR}^{1_{75\%}}$) titrated with A^1 in deionized water (DIW) with (b) exponential decay of the phenanthrene fluorescence as a function of the concentration of A^1 and (c) fluorescence spectra of Al_2O_3 -($\text{PAR}^{3_{25\%}}$ $\text{PAR}^{1_{75\%}}$) titrated with A^2 in DIW with (d) a plot of the quenched phenanthrene fluorescence vs. increasing perylene fluorescence as a function of the concentration of A^2 ($\lambda_{\text{ext}} = 300$ nm).

In a next level of complexity we investigated the interaction of the first shell NPs Al_2O_3 -($\text{PAR}^{2_{5\%}}$ $\text{PAR}^{3_{25\%}}$ $\text{PAR}^{1_{70\%}}$) with A^1 and A^2 leading to the formation of the mixed hybrid architectures $[\text{Al}_2\text{O}_3$ -($\text{PAR}^{2_{5\%}}$ $\text{PAR}^{3_{25\%}}$ $\text{PAR}^{1_{70\%}})]\text{A}^1$ and $[\text{Al}_2\text{O}_3$ -($\text{PAR}^{2_{5\%}}$ $\text{PAR}^{3_{25\%}}$ $\text{PAR}^{1_{70\%}})]\text{A}^2$, respectively. The fluorescence spectrum of the parent Al_2O_3 -($\text{PAR}^{2_{5\%}}$ $\text{PAR}^{3_{25\%}}$ $\text{PAR}^{1_{70\%}}$) NPs exhibits a broad excimer-band around $\lambda = 413$ nm. This band is due to π -stacking interactions of pyrene-pyrene units, or phenanthrene-pyrene units onto the aluminum oxide surface. Figure 7a displays the fluorescence spectra of Al_2O_3 -($\text{PAR}^{2_{5\%}}$ $\text{PAR}^{3_{25\%}}$ $\text{PAR}^{1_{70\%}}$) during the titration with A^1 ($\lambda_{\text{ext}} = 300$ nm). The initial quenching efficiency is very pronounced, whereas during the later course of the titration only slight changes are observed (see Fig. 7b). In the corresponding case of the titration with A^2 the fluorescence-quenching of the mono- and excimer bands is much more moderate and also the emergence of perylene fluorescence is less pronounced. All three first-shell hybrids (Al_2O_3 -($\text{PAR}^{2_{5\%}}$ $\text{PAR}^{3_{25\%}}$ $\text{PAR}^{1_{95\%}})$ / Al_2O_3 -($\text{PAR}^{3_{25\%}}$ $\text{PAR}^{1_{75\%}})$ / Al_2O_3 -($\text{PAR}^{2_{5\%}}$ $\text{PAR}^{3_{25\%}}$ $\text{PAR}^{1_{70\%}})$) showed similar changes of the fluorescence properties as a function of $\text{A}^{1,2}$ -addition, which allowed for a good comparability and reproducibility.

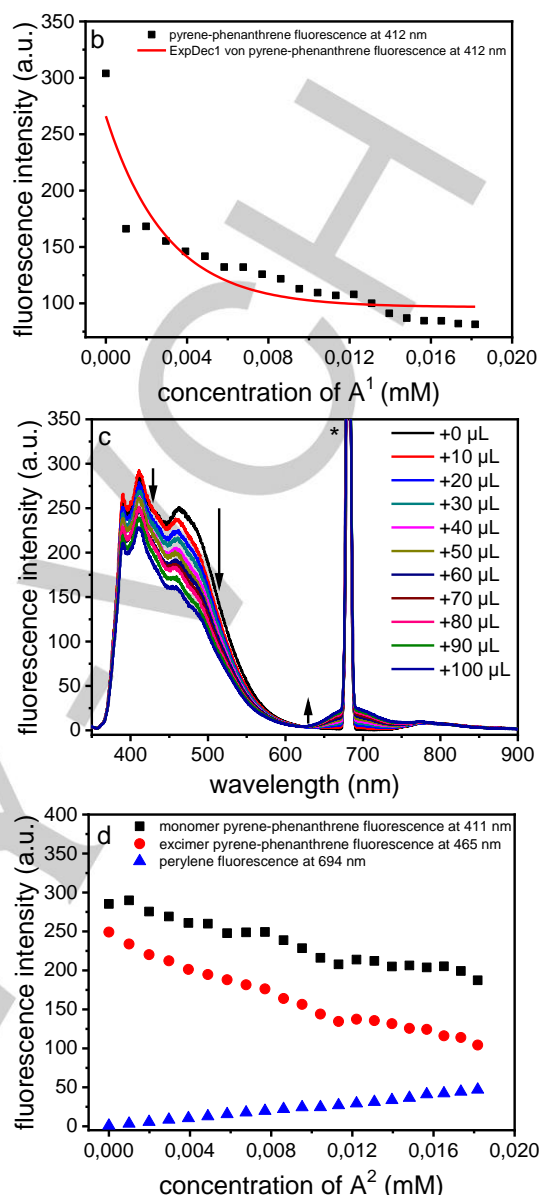
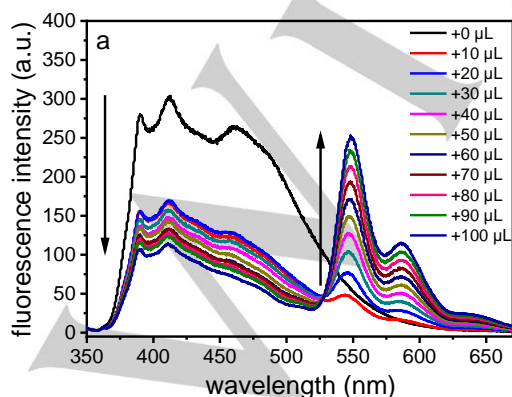


Figure 7. (a) Fluorescence spectra of Al_2O_3 -($\text{PAR}^{2_{5\%}}$ $\text{PAR}^{3_{25\%}}$ $\text{PAR}^{1_{70\%}}$) titrated with A^1 in deionized water (DIW) with (b) exponential decay of the fluorescence-maximum as a function of the concentration of A^1 and (c) fluorescence measurements of Al_2O_3 -($\text{PAR}^{2_{5\%}}$ $\text{PAR}^{3_{25\%}}$ $\text{PAR}^{1_{70\%}}$) titrated with A^2 in DIW with (d) plots of the quenched monomer and excimer fluorescence vs. increasing perylene fluorescence as a function of the concentration of A^2 ($\lambda_{\text{ext}} = 300$ nm).

In order to generate related fluorophilic hybrid NPs we employed the amphiphilic building block A^3 to form the second ligand shell leading to $[\text{Al}_2\text{O}_3$ -($\text{PAR}^{4_{5\%}}$ $\text{PAR}^{1_{95\%}})]\text{A}^3$ (Scheme 4). A^3 consists of a long fluorocarbon tail and a lipophilic part terminated by a pyrene chromophore. The amphiphile is very soluble in both, hydrocarbons and fluorocarbons and exhibits a strong fluorescence at $\lambda_{\text{max}} = 388$ nm. The first shell NPs Al_2O_3 -($\text{PAR}^{4_{5\%}}$ $\text{PAR}^{1_{95\%}}$) contain a fullerene chromophore which can serve as an electron-acceptor. These mono-shell NP precursors are well dispersible in toluene. During the treatment with A^3 forming the second non-covalently bound shell, the dispersibility of the initially lipophilic/fluorophobic nanoparticles switched from hydrocarbons

FULL PAPER

to fluorocarbons. In the target architecture $[\text{Al}_2\text{O}_3-(\text{PAR}^{4.5\%} \text{PAR}^{1.95\%})\text{A}^3]$, A^3 forms a micellar arrangement with the fluorocarbon tails pointing outward to the hexafluorobenzene phase. As a consequence, the second shell contains an inner layer of electron-rich pyrene moieties whereas the first shell is equipped with the electron poor fullerene providing a highly integrated supramolecular donor-acceptor construct. The entire double shell architecture exhibits long-term stability, which was figured out by long term UV-Vis measurements (see Supporting Information Figure S9). In Figure 8a the UV-Vis spectrum of the mono-shell hybrids $\text{Al}_2\text{O}_3-(\text{PAR}^{4.5\%} \text{PAR}^{1.95\%})$ is displayed. The absorption maximum at $\lambda_{\text{max}} = 335$ nm is due to the fullerene cores. It is superimposed by the absorption of the pyrene-moiety at $\lambda_{\text{max}} = 340$ nm of the second-shell hybrids $[\text{Al}_2\text{O}_3-(\text{PAR}^{4.5\%} \text{PAR}^{1.95\%})\text{A}^3]$. The polarity umpolung caused by the binding of amphiphile A^3 is accompanied by presence of a fluorescence signal of the pyrene-unit. Figure 10b represents the appearance of the fluorescence signal of the $[\text{Al}_2\text{O}_3-(\text{PAR}^{4.5\%} \text{PAR}^{1.95\%})\text{A}^3]$ NPs due to the supramolecular binding of A^3 in hexafluorobenzene. It also becomes evident that no dimerization (excimer formation) of the pyrenes takes place because no typically excimer band could be seen in the fluorescence spectra. This implies a rather homogeneous coverage of the second ligand shell with A^3 .

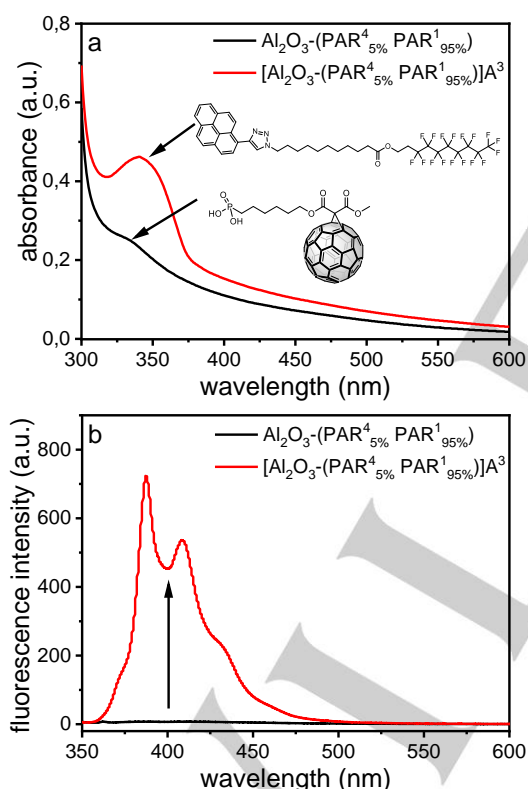


Figure 8. (a) UV-Vis and (b) fluorescence spectra of $\text{Al}_2\text{O}_3-(\text{PAR}^{4.5\%} \text{PAR}^{1.95\%})$ and $[\text{Al}_2\text{O}_3-(\text{PAR}^{4.5\%} \text{PAR}^{1.95\%})\text{A}^3]$ NPs in hexafluorobenzene ($\lambda_{\text{ext}} = 340$ nm).

Figure 9 provides visualization of the polarity umpolung by turning the mono-shell NPs $\text{Al}_2\text{O}_3-(\text{PAR}^{4.5\%} \text{PAR}^{1.95\%})$ to the second shell NPs $[\text{Al}_2\text{O}_3-(\text{PAR}^{4.5\%} \text{PAR}^{1.95\%})\text{A}^3]$ from lipophilic to fluorophilic. $\text{Al}_2\text{O}_3-(\text{PAR}^{4.5\%} \text{PAR}^{1.95\%})$ particles are dispersible in toluene (upper phase) and after addition of A^3 they become dispersible in hexafluorobenzene (lower phase). The NPs were brownish-

colored, caused by the C_{60} -moiety in PAR^4 . The fluorescence of A^3 appeared under UV-light (see Figure 9b).

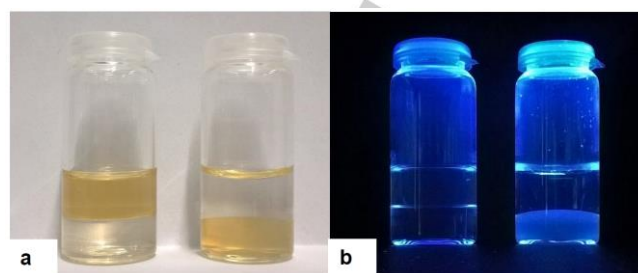


Figure 9. Dispersibility behaviour and optical properties of $\text{Al}_2\text{O}_3-(\text{PAR}^{4.5\%} \text{PAR}^{1.95\%})$ in toluene (upper phase) and the *shell-by-shell* system $[\text{Al}_2\text{O}_3-(\text{PAR}^{4.5\%} \text{PAR}^{1.95\%})\text{A}^3]$ in hexafluorobenzene (lower phase) (a) under day-light and (b) under UV-light.

Conclusions

We reported on a first series of examples for confined space interactions of electron-rich and electron-poor molecules organized in an internal corona of *shell-by-shell* (*SbS*)-structured Al_2O_3 -NP-hybrids. The assembly concept of the corresponding hierarchical architectures relies on both covalent grafting of phosphonic acids on the NPs surface (SAMs formation) and exohedral interdigitation of orthogonal amphiphiles as second ligand layer driven by solvophobic interactions. The electronic communication between the chromophores of different electron demand, such as pyrenes, PDIs (with and without pyridinium-bromide headgroups) and fullerenes was promoted at the layer interface. We have demonstrated that the efficient construction principle of the bilayer hybrids assembled around the electronically “innocent” Al_2O_3 core is robust enough to achieve control over electronic communication between electron-donors and -acceptors in the interlayer region. The electronic communication between the electron-accepting and electron-donating moieties approaching each other at the layer interface were monitored by fluorescence measurements. It was figured out, that the fluorescence of electron donors could be quenched successively by addition of electron acceptors, which confirm the successful electronic communication between electron-donors and -acceptors in the confined layer interface. This *SbS*-concept is very flexible and in principle allows for the construction of limitless structural variants by changing the nature and the permutations of the inorganic core and the functional first- and second layer ligands. Next to electronic communication also other supramolecular processes such as switching, chemical reactions and catalysis are attractive targets for related confined space investigations. Systematic studies towards these challenging goals are currently underway in our laboratory.

Experimental Section

General Methods and Procedures

Aluminium oxide (Al_2O_3) nanoparticles were purchased from Sigma Aldrich (CAS 1344-28-1) as 20wt% dispersions in isopropanol. With BET measurements a specific surface area (SSA) of 108,8 m^2/g and a diameter

FULL PAPER

size of 14 nm was obtained (see Supporting Information). For the functionalization procedure 7.5 mL of a 0.25wt% Al₂O₃ nanoparticle dispersion in isopropanol was mixed with the desired phosphonic acid solution (5 mM) in 5 mL of a 1:1 mixture of MeOH/toluene. The so prepared 0.15wt% nanoparticle dispersions were sonicated for 30 min. After that, the nanoparticle mixtures were washed three times. Washing included centrifugation (10 min, 12.000 rpm), redispersion with sonication in isopropanol and finally into the desired solvent.

Shell-by-shell functionalization of first-shell NPs with amphiphiles driven by solvophobic interactions:

In a typical experiment, the amphiphiles A¹ and A² were dissolved in 0.015wt% phosphonic acid-functionalized Al₂O₃ nanoparticle dispersions, resulting in 0.2 mM concentrations of A¹ and A². These dispersions were titrated in 10 µL steps to 2 mL 0.015wt% phosphonic acid-functionalized nanoparticle dispersions, to make sure that the all-in-all concentration of first-shell functionalized Al₂O₃ nanoparticles and phosphonic-acid derivative was constant during the titration experiments and just the amphiphile concentrations A¹/A² varied. For the system, that involves amphiphile A³, different ratios of 0.015wt% of first-shell functionalized nanoparticles were mixed with second-shell functionalized nanoparticles containing 10% A³.

For UV-Vis, Emission, zeta-potential and DLS measurements, the particle dispersions were measured in 0.015wt% nanoparticle dispersions. For TGA und IR measurements the nanoparticle dispersions were centrifuged, and dried in an oven at 75 °C overnight.

More detailed information about the experimental procedures and methods could be obtained from the Supporting Information.

first-shell system	Al ₂ O ₃ - (PAR ² _{5%} PAR ¹ _{95%})	Al ₂ O ₃ - (PAR ³ _{25%} PAR ¹ _{75%})	Al ₂ O ₃ - (PAR ² _{5%} PAR ³ _{25%} PAR ¹ _{70%})	Al ₂ O ₃ - (PAR ⁴ _{5%} PAR ¹ _{95%})
conc. of chromophore used for first-shell functionalization (mM)	0.25	1.25	1.5	0.25
conc. of spacing-SAM (C ₁₆ -PA) (mM)	4.75	3.75	3.5	4.75
conc. of second-shell chromophore (mM) A ^{1/2} , DDPB / A ³				
+0 µL /0%	0	0	0	0
+10 µL /1%	9.950E-4	9.950E-4	9.950E-4	0.00625
+20 µL /2%	0.00198	0.00198	0.00198	0.01250
+30 µL /3%	0.00296	0.00296	0.00296	0.01875
+40 µL /4%	0.00392	0.00392	0.00392	0.02500
+50 µL /5%	0.00488	0.00488	0.00488	0.03125
+60 µL /6%	0.00583	0.00583	0.00583	0.03750
+70 µL /7%	0.00676	0.00676	0.00676	0.04375
+80 µL /8%	0.00769	0.00769	0.00769	0.05000
+90 µL /9%	0.00861	0.00861	0.00861	0.05625
+100 µL /10%	0.00952	0.00952	0.00952	0.06250

Acknowledgements

We thank the Cluster of Excellence "Engineering of Advanced Materials" (EAM), funded by the German Research Council (DFG) and the Graduate School Advanced Materials and Processes (GS AMP) for financial support. We also thank the Chair of Chemical Reaction Engineering (CRT) in Erlangen for the BET measurement.

Keywords: nanoparticles • *shell-by-shell* architectures • confined space • electronic communication • micelles

- [1] a) L. Zeininger, S. Petzi, J. Schönamsgruber, L. Portilla, M. Halik, A. Hirsch, *Chem. Eur. J.* **2015**, *21*, 14030-14035; b) L. Zeininger, L. M. S. Stiegler, L. Portilla, M. Halik, A. Hirsch, *ChemistryOpen* **2018**, *7*, 282-287; c) T. Luchs, M. Sarcletti, L. Zeininger, L. Portilla, C. Fischer, S. Harder, M. Halik, A. Hirsch, *Chem. Eur. J.* **2018**, *24*, 13589-13595; d) S. Klein, L. M. S. Stiegler, C. Harreiss, L. V. R. Distel, W. Neuhuber, E. Spiecker, A. Hirsch, C. Kryschi, *ACS Applied Bio Materials* **2018**, *1*, 2002-2011.
- [2] a) T. Kondo, R. Yamada, K. Uosaki, *Fundamentals and Applications*, Wiley-VCH, Weinheim **2013**, 7-42; b) H. Dietrich, T. Schmaltz, M. Halik, D. Zahn, *Phys. Chem. Chem. Phys.* **2017**, *19*, 5137-5144; c) S. P. Pujari, L. Scheres, A. T. Marcellis, H. Zuilhof, *Angew. Chem. Int. Ed. Engl.* **2014**, *53*, 6322-6356; d) I. Levine, S. M. Weber, Y. Feldman, T. Bendikov, H. Cohen, D. Cahen, A. Vilan, *Langmuir* **2012**, *28*, 404-415.
- [3] T. Pellegrino, L. Manna, S. Kudera, T. Liedl, D. Koktysh, A. L. Rogach, S. Keller, J. Rädler, G. Natile, W. J. Parak, *J. Am. Chem. Soc.* **2004**, *4*, 703-707.
- [4] a) G. Decher, *Science* **1997**, *277*, 1232-1237; b) G. Decher, M. Eckle, J. Schmitt, B. Struth, *Curr. Opin. Colloid Interface Sci.* **1998**, *3*, 32-39.
- [5] J. E. Wittmann, L. M. S. Stiegler, C. Henkel, J. Träg, K. Götz, T. Unruh, D. Zahn, A. Hirsch, D. Guldi, M. Halik, *Adv. Mater. Interfaces* **2019**.
- [6] a) L. J. Andrews, *Chem. Rev.* **1954**, *54*, 713-776; b) R. Foster, *J. Phys. Chem.* **1980**, *84*, 2135-2141.
- [7] M. Kellermann, W. Bauer, A. Hirsch, B. Schade, K. Ludwig, C. Böttcher, *Angew. Chem. Int. Ed.* **2004**, *43*, 2959-2962.
- [8] a) M. Voigt, M. Klaumünzer, A. Ebel, F. Werner, G. Yang, R. Marczak, E. Spiecker, D. M. Guldi, A. Hirsch, W. Peukert, *J. Phys. Chem. C* **2011**, *115*, 5561-5565; b) C. D. Schmidt, C. Böttcher, A. Hirsch, *Eur. J. Org. Chem.* **2007**, *2007*, 5497-5505; c) J. Schönamsgruber, B. Schade, R. Kirschbaum, J. Li, W. Bauer, C. Böttcher, T. Drewello, A. Hirsch, *Eur. J. Org. Chem.* **2012**, *2012*, 6179-6186.
- [9] a) L. Delain-Bioton, D. Villemin, J.-F. Lohier, J. Sopkova, P.-A. Jaffrès, *Tetrahedron* **2007**, *63*, 9677-9684; b) S. H. Etschel, L. Portilla, J. Kirschner, M. Drost, F. Tu, H. Marbach, R. R. Tykwinski, M. Halik, *Angew. Chem. Int. Ed.* **2015**, *54*, 9235-9238.
- [10] a) A. W. Coats, J. P. Redfern, *Analyst* **1963**, *88*, 906-924; b) C. D. Doyle, *J. Appl. Polym. Sci.* **1961**, *5*, 285-292.
- [11] a) L. Zeininger, M. Klaumünzer, W. Peukert, A. Hirsch, *Int. J. Mol. Sci.* **2015**, *16*, 8186-8200; b) L. Zeininger, L. Portilla, M. Halik, A. Hirsch, *Chem. Eur. J.* **2016**, *22*, 13506-13512.
- [12] a) H. Klauk, U. Zschieschang, J. Pflaum, M. Halik, *Nature* **2007**, *445*, 745-748; b) L. F. P. Berlanga, Friedrich-Alexander University Erlangen-Nuremberg (Erlangen), **2017**.
- [13] a) M. I. Sluch, I. D. W. Samuel, M. C. Petty, *Chem. Phys. Lett.* **1997**, *280*, 315-320; b) K. Datta, A. K. Mukherjee, *Spectrochim. Acta, Part A* **2006**, *65*, 261-264.
- [14] K. Datta, M. Banerjee, B. K. Seal, A. K. Mukherjee, *J. Chem. Soc., Perkin Trans. 2* **2000**, 531-534.
- [15] a) Y. Zhong, M. T. Trinh, R. Chen, W. Wang, P. P. Khlyabich, B. Kumar, Q. Xu, C. Y. Nam, M. Y. Sfeir, C. Black, M. L. Steigerwald, Y. L. Loo, S. Xiao, F. Ng, X. Y. Zhu, C. Nuckolls, *J. Am. Chem. Soc.* **2014**, *136*, 15215-15221; b) Y. Lin, Y. Wang, J. Wang, J. Hou, Y. Li, D. Zhu, X. Zhan, *Adv. Mater.* **2014**, *26*, 5137-5142; c) Y.

FULL PAPER

- Cai, L. Huo, X. Sun, D. Wei, M. Tang, Y. Sun, *Adv. Energy Mater.* **2015**, *5*.
- [16] L. Zhong, F. Xing, W. Shi, L. Yan, L. Xie, S. Zhu, *ACS Appl. Mater. Interfaces* **2013**, *5*, 3401-3407.
- [17] a) B. J. Coe, *Acc. Chem. Res.* **2006**, *29*, 383-393; b) R. C. Vieira, D. E. Falvey, *J. Am. Chem. Soc.* **2008**, *130*, 1552-1553; c) D. Behar, P. Neta, C. Schultheisz, *J. Phys. Chem. A* **2002**, *106*, 3139-3147; d) A. Skrzypczak, P. Neta, *J. Phys. Chem. A* **2003**, *107*, 7800-7803; e) A. G. Peroff, E. Weitz, R. P. Van Duyne, *Phys. Chem. Chem. Phys.* **2016**, *18*, 1578-1586; f) M. Z. Ertem, S. J. Konezny, C. M. Araujo, V. S. Batista, *J. Phys. Chem. Lett.* **2013**, *4*, 745-748; g) Y. Yan, E. L. Zeitler, J. Gu, Y. Hu, A. B. Bocarsly, *J. Am. Chem. Soc.* **2013**, *135*, 14020-14023.
- [18] a) D. A. Wade, S. A. Tucker, *Talanta* **2000**, *53*, 571-578; b) D. A. Wade, C. Mao, A. C. Hollenbeck, S. A. Tucker, *Frenzius J. Anal. Chem.* **2001**, *369*, 378-384; c) S. Pandey, J. William E. Acree, J. C. Fetzer, *Talanta* **1997**, *45*, 39-45; d) S. Pandey, J. William E. Acree, J. C. Fetzer, *Talanta* **1998**, *47*, 769-778; e) S. Pandey, W. E. A. Jr., J. C. Fetzer, *Mikrochim. Acta* **1998**, *129*, 41-45.
- [19] a) M. G. Uddin, A. T. M. Z. Azam, *Am. J. Biochem. Mol. Biol.* **2013**, *3*, 175-181; b) J. B. Birks, L. G. Christophorou, *Spectrochim. Acta* **1962**, *19*, 401-410; c) C. E. Agudelo-Morales, R. E. Galian, J. Pérez-Prieto, *Anal. Chem.* **2012**, *84*, 8083-8087.
- [20] a) F. Würthner, T. E. Kaiser, C. R. Saha-Möller, *Angew. Chem. Int. Ed.* **2011**, *50*, 3376-3410; b) F. Würthner, C. R. Saha-Moller, B. Fimmel, S. Ogi, P. Leowanawat, D. Schmidt, *Chem. Rev.* **2016**, *116*, 962-1052.

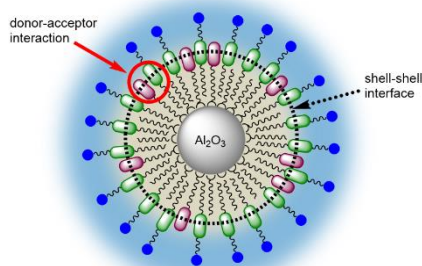
FULL PAPER

Entry for the Table of Contents (Please choose one layout)

Layout 1:

FULL PAPER

Construction of *shell-by-shell* functionalized Al_2O_3 NPs with a sophisticated push-pull system in a confined space of the *shell-shell* interface with concomitant changing fluorescence features of the system.



Lisa. M. S. Stiegler, and Andreas Hirsch*

Page No. – Page No.

Electronic Communication in Confined Space Coronas of *Shell-by-Shell* Structured Al_2O_3 -Nanoparticle Hybrids Containing Two Layers of Functional Organic Ligands